energies

MDPI

Article

A Study of the Influence of Fin Parameters on Porous-Medium Approximation

Junjie Tong [1,*], Shuming Li [2], Tingyu Wang [1,*], Shuxiang Wang [1], Hu Xu [1] and Shuiyu Yan [1]

[1] School of Naval Architecture and Ocean Engineering, Guangzhou Maritime University, Guangzhou 510700, China
[2] School of Materials and Energy, Guangdong University of Technology, Guangzhou 511400, China
* Correspondence: junjietong@gzmtu.edu.cn (J.T.); wangtingyu825@126.com (T.W.); Tel.: +86-189-2220-9152 (J.T.)

Abstract: The porous-medium approximation (PM) approach is extensively employed in large-quantity grid simulations of heat exchangers, providing a time-saving approach in engineering applications. To further investigate the influence of different geometries on the implementation of the PM approach, we reviewed existing experimental conditions and performed numerical simulations on both straight fins and serrated fins. Equivalent flow and heat-transfer factors were obtained from the actual model, and computational errors in flow and heat transfer were compared between the actual model and its PM model counterpart. This exploration involved parameters such as aspect ratio (a^*), specific surface area (A_{sf}), and porosity (γ) to evaluate the influence of various geometric structures on the PM approach. Whether in laminar or turbulent-flow regimes, when the aspect ratio a^* of straight fins is 0.98, the flow error (δ_f) utilizing the PM approach exceeds 45%, while the error remains within 5% when a^* is 0.05. Similarly, for serrated fins, the flow error peaks (δ_f > 25%) at higher aspect ratios (a^* = 0.61) with the PM method and reaches a minimum (δ_f < 5%) at lower aspect ratios (a^* = 0.19). Under the same Reynolds numbers (Re), employing the PM approach results in an increased heat-transfer error (δ_h)with rising porosity (γ) and decreasing specific surface area (A_{sf}), both of which remained under 10% within the range of this study. At lower aspect ratios (a^*), the fin structure becomes more compact, resulting in a larger specific surface area (A_{sf}) and smaller porosity (γ). This promotes more uniform flow and heat transfer within the model, which is closer to the characteristics of PM. In summary, for straight fins at $0 < a^* < 0.17$ in the laminar regime ($200 < Re < 1000$) and in the turbulent regime ($1200 < Re < 5000$) and for serrated fins at $0 < a^* < 0.28$ in the laminar regime ($400 < Re < 1000$) or $0 < a^* < 0.32$, in the turbulent regime ($2000 < Re < 5000$), the flow and heat-transfer errors are less than 15%.

Keywords: straight fins; serrated fins; aspect ratio; specific surface area; porous-medium approximation

Citation: Tong, J.; Li, S.; Wang, T.; Wang, S.; Xu, H.; Yan, S. A Study of the Influence of Fin Parameters on Porous-Medium Approximation. *Energies* **2024**, *17*, 1133. https://doi.org/10.3390/en17051133

Academic Editor: Artur Blaszczuk

Received: 8 January 2024
Revised: 9 February 2024
Accepted: 18 February 2024
Published: 27 February 2024

1. Introduction

Compact heat exchangers are widely employed in various industries such as aerospace applications [1,2], nuclear power plants [3], the automotive industry [4], hydrogen energy [5], refrigeration [6], and concentrated solar power [7,8] due to their compact structure and high heat-transfer efficiency. Yang Jie [9] mentioned that there are four main modeling approaches used for numerical simulation: the unit model, the periodic model, the porous model, and the whole model. The results of the study showed that the unit model and the periodic model neglected the effects of inlets and outlets, and the pressure drop calculated by multiplying the pressure drop of each unit or periodical region by the number of repetitions differed significantly from the experimental data. The pressure drop in the unit flow channel is approximately 20% smaller than the experimental data, and the pressure drop in the periodic model is approximately 40% larger than the experimental data, indicating that the unit and periodic models do not directly predict pressure drop. The porous model

and the whole model have high accuracy in predicting heat transfer, pressure drop, and overall performance but the porous model requires additional experimental correlations or correlation simulations to obtain the parameters of the porous medium; the whole model requires large computational resources [10,11].

The PM approach offers a unique advantage in simplifying complex geometric structures. As early as the 1970s, Patankar and Spalding [12,13] introduced the concept of distributed resistance to solve flow fields and enthalpy distribution in steam generators. This method was initially proposed for modeling shell-and-tube heat exchangers, allowing resistance losses due to the presence of internal solids to be considered as a uniformly distributed resistance applied to the flow and heat transfer of the heat exchanger, without the need to model any of its specific details. This effectively addresses the computational challenges associated with simulating the entire model, permitting the use of a coarser grid than what a complete geometric model would require. Since its inception, the PM approach has been employed to analyze various geometric shapes, including turbine engines [14], wind tunnels [15], agricultural products [16], tube bundles [17,18], and heat exchangers [19,20].

Especially in the large-quantity grid simulation of various heat exchangers for different purposes, the following examples confirm that the PM approach ensures computational accuracy with fewer computational resources. Li [21] simplified the finned area on the tube surface to a ring-shaped PM zone using the PM approach, and the relative error of the predicted pressure drop was less than 10% compared with the experimental values. Zhu [22] systematically compared the performance of actual models and the PM approach for compact plate–fin heat exchangers with different numbers of channels. This verified that the accuracy of the PM approach increases as the number of channels increases, and for heat exchangers with over 30 channels, it can predict not only the overall pressure drop but also detailed pressure and velocity distributions with errors within 10%.

The PM approach holds significant potential for large-quantity grid simulations of heat exchangers. However, there has been limited systematic exploration by researchers into the influencing factors of this approach. As mentioned by Lage and Antohe [23], it is necessary to investigate how the geometric shapes of PM influence form–drag effects. L. Wilson [24] conducted a detailed study on the impact of flow parameters Re, geometric parameters, and the number of rods on the dimensionless pressure drop in experimental models. This study confirmed that variations in the form–drag related to flow, fin height (h), and fin spacing (s) are the reasons for the variations in pressure drop between the different models. The aspect ratio (a^*) represents the s to h ratio of a rectangular channel, reflecting the combined influence on the channel cross-section, and is utilized in numerous analytical expressions for rectangular channels. Therefore, for a systematic exploration of the effects brought about by geometric structures, investigating the impact of the aspect ratio (a^*) becomes crucial. Furthermore, while there is considerable literature discussing flow issues, there is comparatively less discussion regarding heat transfer involving the PM method. Huang [25] mentioned that due to the thermal-equilibrium method in PM models relying solely on the porosity (γ) parameter to determine heat transfer, the heat-transfer errors are larger than the flow errors. Therefore, some researchers, such as Zhu, Huang, and Li [21,22,26], use the PM approach primarily for fluid dynamics analysis while avoiding discussions about the equivalent heat transfer. Nevertheless, the non-thermal-equilibrium method can be used to determine the heat transfer in an equivalent porous medium by adjusting the specific surface area (A_{sf}) and the interfacial heat-transfer coefficient (h_{fs}).

Based on the above literature, it is necessary to systematically explore the influencing factors of flow and heat transfer in the PM approach. Therefore, this paper conducts a validation analysis of the PM approach applied to both straight fins and serrated fins in compact heat exchangers. It also explores the influence of various geometric parameters, including the aspect ratio (a^*), specific surface area (A_{sf}), and porosity (γ), for the PM approach under varying flow conditions. The ultimate goal is to establish a reference range

for the equivalent simulation of compact heat exchangers. The specific objectives of this study can be summarized as follows:

- To verify the accuracy of the PM approach in equivalently simulated fluid-flow and heat-transfer processes for straight fins and serrated fins by comparison with experimental results;
- To quantify the efficiency of the PM approach in saving computational time by comparing the simulation computation time;
- To explore the influence of the fin aspect ratio (a^*) and different flow conditions (Re) on the flow calculations with the PM approach;
- To explore the influence of the afin-specific surface area (A_{sf}) and porosity (γ) on the heat-transfer calculations with the PM approach.

2. Numerical Simulation

2.1. Physical Model

Segments of both straight-fin channels and serrated-fin channels were chosen as the objects of study. The geometry of the straight fins and serrated fins are shown in Figure 1. The straight fins with a^* = 0.17 and serrated fins with a^* = 0.32 have the same geometrical dimensions as the straight fins numbered 11.1 and serrated fins numbered 13.95 in Kays' study [27], which facilitated the validation of the numerical models' reliability. These geometric dimensions meet the requirements for most fin designs [28]. The specific parameters are presented in Table 1. The dimensionless aspect ratio (a^*) was employed to represent the ratio of fin spacing (s) to fin height (h). By designing various combinations of s and h, the aspect ratio (a^*), specific surface area (A_{sf}), and porosity (γ) can be adjusted to explore the impacts of different geometric structures on the PM approach. Because both types of fins exhibit a symmetrical structural distribution, the models can be established and computed using representative unit cells, as illustrated in Figure 1. All the numerical models in this study were computed on a workstation with an 11th Gen Intel (R) Core(TM) i9-11900K CPU.

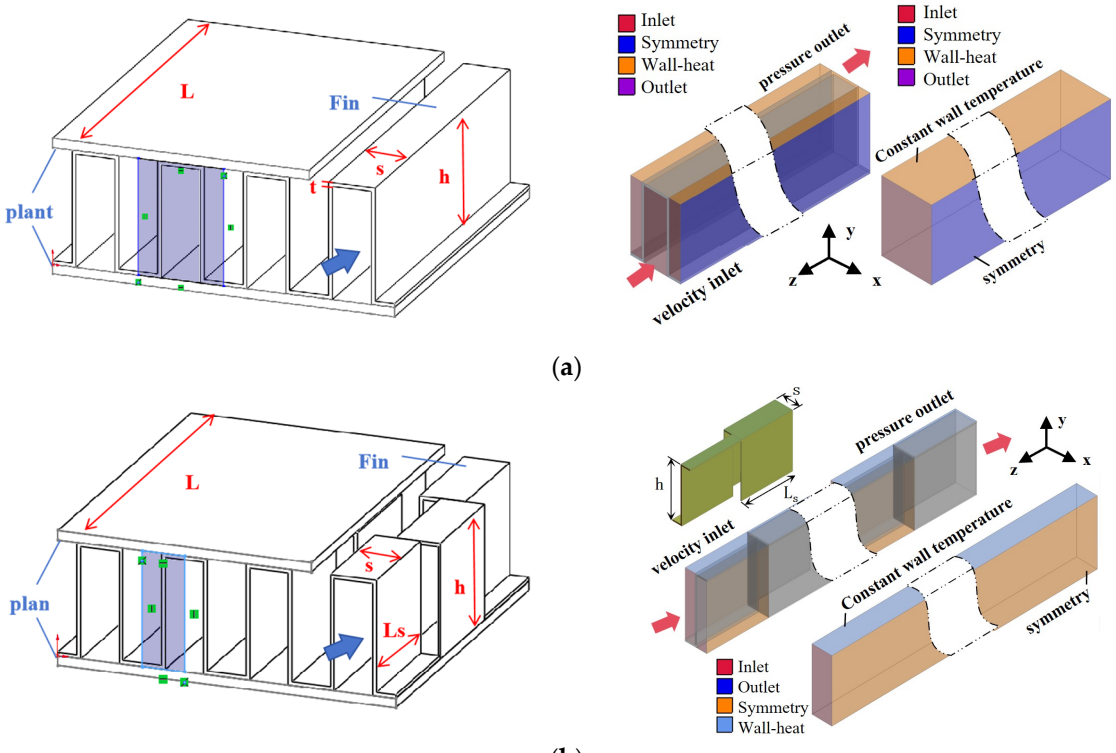

Figure 1. The geometry of the fin: (**a**) Straight fins; (**b**) Serrated fins.

Table 1. Fin geometry parameters.

Fin Type	Aspect Ratio (a^*)	Equivalent Diameter (De/mm)	Specific Surface Area (A_{sf}/m^{-1})	Porosity (γ)
Straight Fins	0.17	3.55	1667	0.91
	0.23	4.55	877	0.93
	0.33	6.02	667	0.95
	0.41	7.09	476	0.96
	0.49	8.04	385	0.97
	0.61	9.21	323	0.97
	0.74	10.35	263	0.98
	0.82	10.99	217	0.98
	0.90	11.56	179	0.98
	0.98	12.09	164	0.98
Serrated Fins	0.19	2.02	1570	0.86
	0.25	2.56	1248	0.89
	0.32	3.09	1029	0.90
	0.38	3.48	906	0.91
	0.44	3.89	804	0.92
	0.50	4.26	727	0.93

The dimensions of the Kays model are as follows: For the straight fins, the fin spacing (s) = 2.286 mm, fin height (h) = 12.19 mm, fin thickness (t) = 0.2 mm, and the total fin length (L) = 203.2 mm. For serrated fins, the fin spacing (s) = 2.04 mm, fin height (h) = 6.35 mm, fin thickness (t) = 0.16 mm, serration length (L_s) = 6.35 mm, and the total fin length (L) = 76.2 mm.

$$a^* = \frac{s-t}{h} = \frac{b}{h} \tag{1}$$

$$A_{fs} = \frac{A}{V_p} \tag{2}$$

$$\gamma = \frac{V_f}{V_p} \tag{3}$$

where a^* is the aspect ratio; s is the fin spacing, mm; t is the fin thickness, mm; h is the fin height, mm; γ is the porosity; V_f is the fluid circulation volume, m^3; V_p is the volume of the porous region, m^3; A_{fs} is the specific surface area (interfacial area density in the fluent operation interface), m^{-1}; and A is the fluid solid interface area, m^2.

2.2. Initial and Boundary Conditions

In Kays' experiments, the fins were made of solid aluminum, and the channels contained incompressible air with consistent material properties. In the simulations, the fluid flows along the negative z-axis, and the inlet conditions were set as the velocity inlet with a constant inlet temperature of 300 K. The outlet was modeled as the pressure outlet, and a coupled-wall boundary condition was applied to equate the thermal conduction rate on the solid inner surface with the convective heat-transfer rate of the fluid on the solid surface. Symmetry boundary conditions were applied to both sides of the domain. The upper and lower sections were subjected to constant wall-temperature conditions of 450 K. Given the computational demands and the nature of the model, this study makes several assumptions based on Kays' experiments [27]:

- The study considers the fin models under stable conditions that reach dynamic equilibrium. Therefore, a steady-state model is employed, assuming homogeneous PM properties within the fin channel;
- The flow characteristics in adjacent channels are remarkably similar, and the fins are symmetrically distributed in the structure. This allows for the selection of representative units with symmetrical boundary conditions for simulation;

- The thickness of the straight plate is significantly smaller than the height of the fins, allowing us to disregard the straight plate's thermal resistance;
- Radiation heat transfer is considered negligible.

The simulations were conducted using Ansys Fluent 2021R1. According to Yang's work [29], the laminar-flow regime ranges from 200 < *Re* < 1000, and the turbulent regime ranges from 1200 < *Re* < 5000. The SIMPLE algorithm was utilized to address the coupling of pressure and velocity in the laminar-flow region, while the SST-k-ω low-Reynolds-number turbulence model [30] was employed for the turbulent flow. A second-order upwind scheme was employed to enhance the accuracy of the governing equations. Convergence is considered achieved when the residuals of the continuity equation, momentum equation, energy equation, turbulence kinetic energy, and turbulence dissipation rate fall below 10^{-8}. As illustrated in Figure 1b, replacing the channel region with the PM model allows for simulating all the straight fins with a coarser grid.

2.3. Governing Equations

2.3.1. Momentum Equation

To simulate the PM model, momentum source terms are incorporated into the standard fluid-flow equations [31]. These source terms encompass both viscous losses (the Darcy term) and inertial losses. In the case of homogeneous PM, the equations take the form of Equation (4).

The calculation of the viscous-resistance coefficient and the inertial-resistance coefficient in the PM method can be obtained not only by using empirical formulas [32–34] but also by fitting a quadratic equation relating the pressure drop to source terms to obtain the relationship between velocity and pressure drop, as shown in Equations (5)–(9). This study uses the above methodology to obtain their corresponding PM-model coefficients through actual model simulations, with different coefficients used for different fin geometries.

$$S_i = -\left(\frac{\mu}{\alpha}v + C_2\frac{1}{2}\rho|v|v\right) \tag{4}$$

$$\nabla p = S_i \tag{5}$$

$$\nabla p = -\left(\frac{\mu}{\alpha}v + C_2\frac{1}{2}\rho|v|v\right) \tag{6}$$

$$\nabla p = Av^2 + Bv \tag{7}$$

$$A = C_2\frac{1}{2}\rho\Delta n \tag{8}$$

$$B = \frac{1}{\alpha}\mu\Delta n \tag{9}$$

where S_i the power -source term; v is the magnitude of the velocity, m·s^{-1}; ρ is the fluid density, kg·m^{-3}; and μ is the power viscosity, kg·(m·s)$^{-1}$. $1/\alpha$ and C_2 are the viscous-drag coefficient and the inertial-drag coefficient, and A and B are the binomial-fitting coefficients. The equivalent drag parameters of the PM model can be obtained by numerical calculation from the above method, these are the viscous-drag coefficient $1/\alpha$ and the inertial-drag coefficient C_2, which are the drag coefficients corresponding to the unit length.

2.3.2. Momentum Equation

To simulate PM, momentum source terms are incorporated into the standard fluid-flow equations. These source terms encompass both viscous losses (the Darcy term) and inertial losses. In the case of a homogeneous PM, the equations take the following form:

$$\frac{\partial}{\partial t}\left(\gamma\rho_f E_f\right) + \nabla\cdot\left(\vec{v}\left(\rho_f E_f + p\right)\right) = \nabla\cdot\left(\gamma k_f \nabla T_f - \left(\sum_i h_i J_i\right) + \left(\overline{\tau}\cdot\vec{v}\right)\right) + S_f^h + h_{fs}A_{fs}\left(T_s - T_f\right) \quad (10)$$

The conservation equation for the solid region is:

$$\frac{\partial}{\partial t}((1-\gamma)\rho_s E_s) = \nabla\cdot((1-\gamma)k_s\nabla T_s) + S_s^h + h_{fs}A_{fs}\left(T_f - T_s\right) \quad (11)$$

where E_f is the total fluid energy, J; E_s is the total solid energy, J; ρ_f is the fluid density, kg-m $^{-3}$; ρ_s is the solid density, kg·m^{-3}; k_f is the fluid thermal conductivity, $W\cdot$ (m·K)$^{-1}$ (including turbulence contribution); k_s is the solid thermal conductivity, $W\cdot$ (m·K)$^{-1}$; h_{fs} is the heat-transfer coefficient at the fluid/solid interface, $W\cdot$(m·K)$^{-1}$; A_{sf} is the interfacial areal density, m^{-1}; A_{sf} the ratio of the area of the liquid–solid interface to the volume of the porous zone; γ is the medium porosity; T_s is the solid temperature, K; T_f is the fluid temperature, K; $S_f{}^h$ is the fluid-enthalpy source term; and $S_f{}^s$ is the solid-enthalpy source term.

3. Model Validation

3.1. Grid-Independence Analysis

To accurately simulate the heat-transfer and flow characteristics, a structured grid was chosen to add boundary layers at the fluid and solid contact surfaces, as shown in Figure 2. The grid was analyzed independently, which ensures model accuracy and reduces the waste of computational resources. This is shown in Table 2.

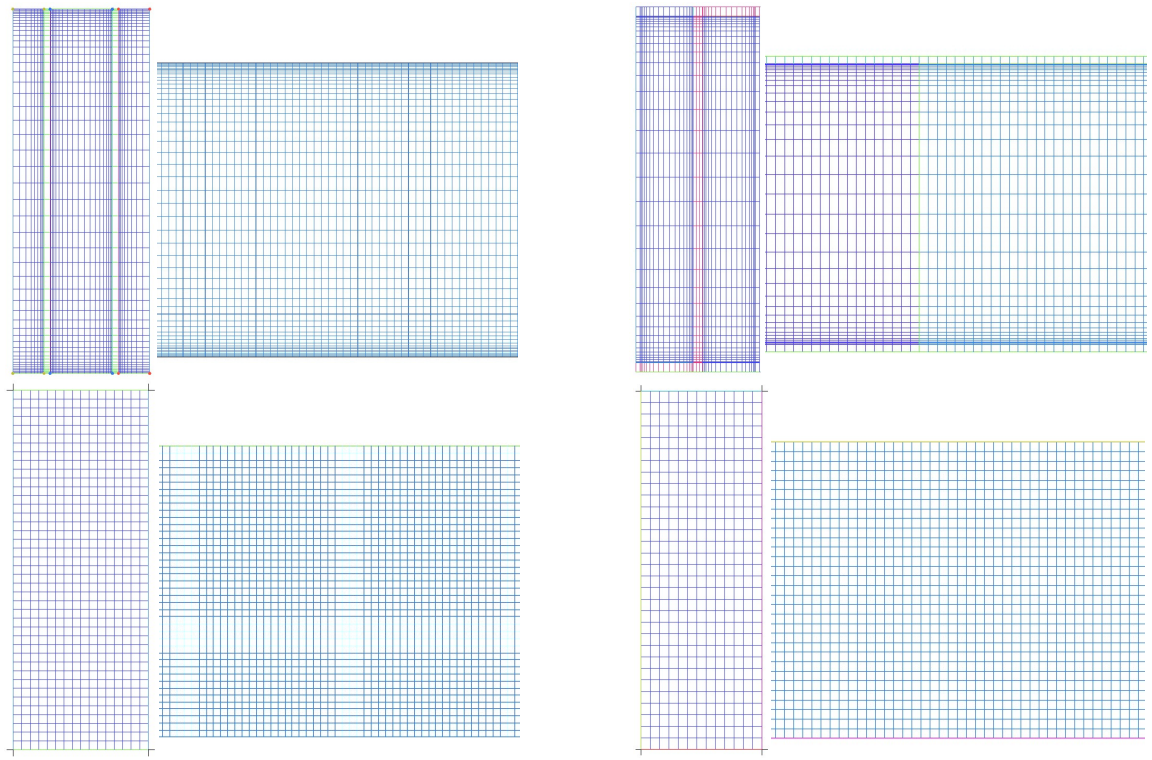

(**a**) (**b**)

Figure 2. Actual model mesh and the PM model mesh: (**a**) Straight fins; (**b**) Serrated fins.

Table 2. Influence of grid size on model stability.

Straight Fins	Relative Error		Serrated Fins	Relative Error	
Number of Grids	Pressure Drop (Pa)	Outlet Temperature (K)	Number of Grids	Pressure Drop (Pa)	Outlet Temperature (K)
254,375	3.2%	1.7%	176,832	2.9%	1.4%
457,603	2.4%	0.9%	328,455	2.3%	0.8%
631,160	0.6%	0.5%	514,384	1.5%	0.6%
1,084,122	0.5%	0.3%	777,769	0.6%	0.1%
1,268,280	−0.1%	0.2%	1,062,318	0.5%	0.2%
1,513,806	0.0%	0.0%	1,266,162	0.0%	0.0%

As the number of grids increased to over 631,160 for the straight fin model and 777,769 for the serrated fin model, the pressure drop and outlet temperature stabilized. The relative errors for the straight fins were approximately ±1% and ±0.5%, respectively, and for the serrated fins, they were approximately ±1% and ±0.1%, respectively. These errors fall within an acceptable range. Grid-independent verification was conducted for all the models in this study, with relative errors within ±1%.

3.2. Model-Reliability Verification

Multiple researchers have cited Kays' [27] experimental data, affirming its reliability. This paper compares the experimental and simulated data for the flow factor f and heat-transfer factor j for straight fins (a^* = 0.17) and serrated fins (a^* = 0.32) under laminar- and turbulent-flow conditions, as illustrated in Figures 2 and 3, where the friction factor f and the heat-transfer factor j are defined as follows:

$$f = \frac{\Delta P}{2\rho u^2}\frac{D_e}{L} \tag{12}$$

$$j = \frac{H}{\rho u C_p} P_r^{\frac{2}{3}} \tag{13}$$

where ΔP is the pressure drop of the fluid in the tube of length L, Pa; u is the mean velocity, m· s^{-1}; D_e is the equivalent diameter, m; H is the convective heat-transfer coefficient, $W\cdot(m^2\cdot s)^{-1}$; C_p is the specific heat of the fluid, $J\cdot(kg\cdot K)^{-1}$.

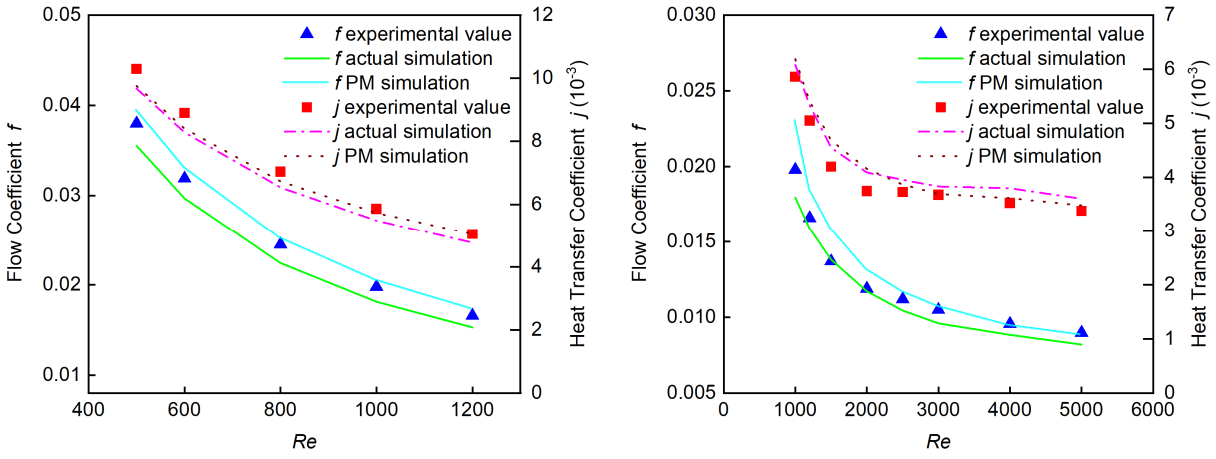

Figure 3. Comparison between the calculated results of the straight fin model and the experimental results in the literature: (**a**) Laminar-flow state; (**b**) Turbulent-flow state.

As can be seen from Figures 3 and 4, it is evident that the simulated and experimental values for the factors f and j exhibit similar trends with Re variation. As shown in Table 3, the maximum relative error between the actual simulation and experimental values was within 7.9%, which indicates that the actual simulation and the experimental results are in perfect agreement and can effectively predict the flow and heat-transfer characteristics of the straight fins and serrated fins. Clearly, the PM simulation shows a significant relative maximum error in the flow factor f compared with the experimental results at a^* = 0.32 for serrated fins. This highlights the necessity of investigating the factors that affect the accuracy of the PM approach.

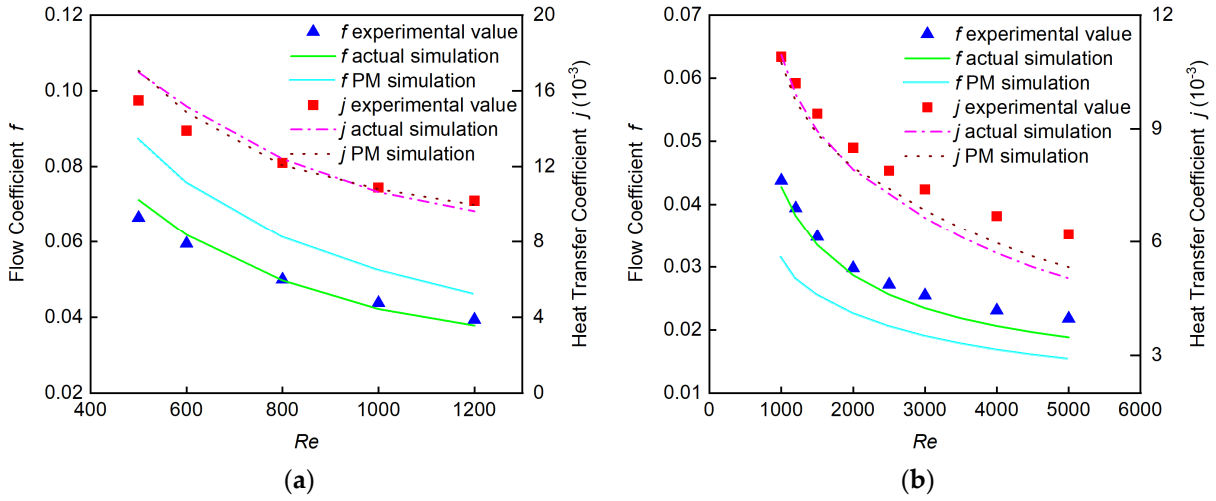

Figure 4. Comparison between the calculated results of the serrated fin model and the experimental results in the literature: (**a**) Laminar-flow state; (**b**) Turbulent-flow state.

Table 3. Relative error between simulated and experimental values.

Fin Type	Flow State	Maximum Relative Error between Actual Simulation and Experimental		Maximum Relative Error between PM Simulation and Experimental	
		Flow Factor f	Heat-Transfer Factor j	Flow Factor f	Heat-Transfer Factor j
Straight Fins	Laminar	7.9%	6.1%	3.9%	4.5%
	Turbulent	7.6%	6.3%	4.4%	3.5%
Serrated Fins	Laminar	5.6%	5.4%	15.0%	3.3%
	Turbulent	5.4%	7.6%	14.6%	5.2%

3.3. Performance-Verification Analysis

We investigated the impact of different geometric parameters on fin performance and to analyze the effects of aspect ratio (a^*) and specific surface area (A_{sf}) on the pressure drop and outlet temperature for both fins under different flow conditions; the numerical results are presented in Figure 5. The pressure distribution essentially determines the flow distribution, which, in turn, affects the heat exchanger's performance.

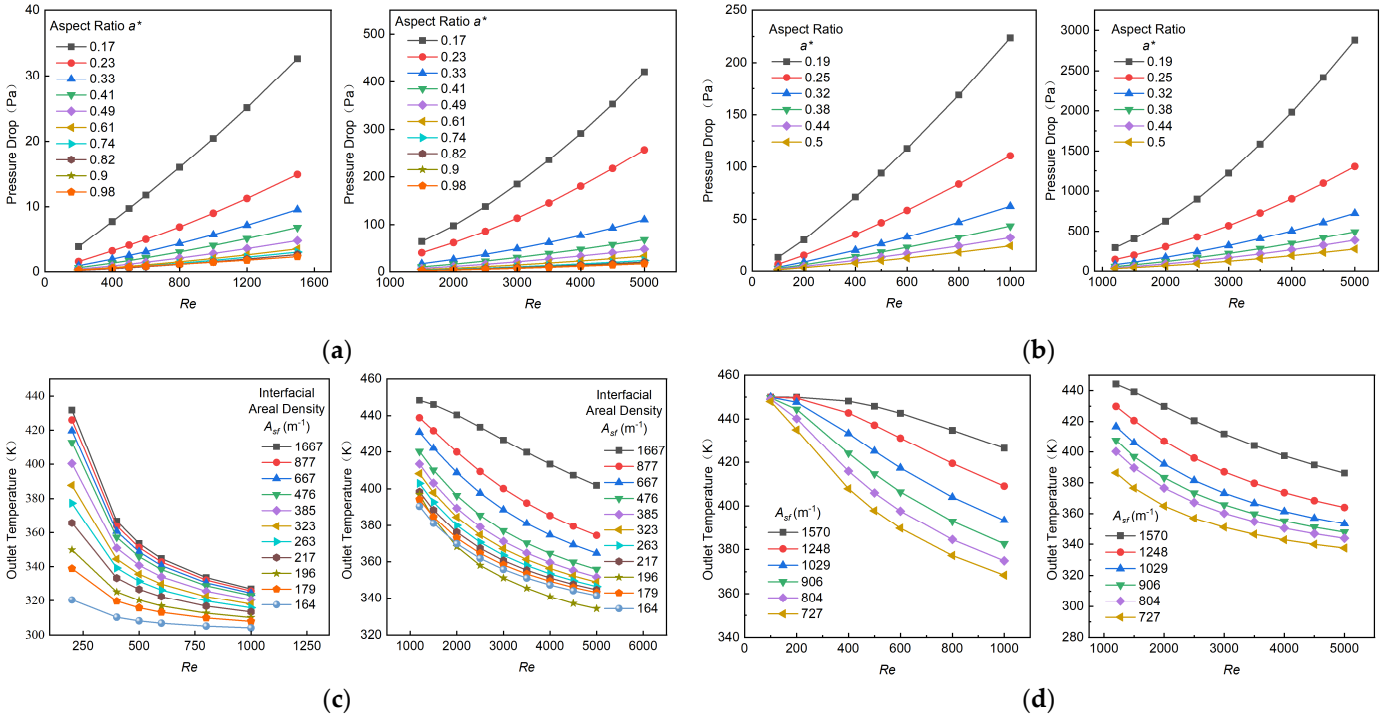

Figure 5. Influence of different fin geometries: (**a**) Influence of different a^* values of straight fins on pressure drop; (**b**) Influence of different a^* values of serrated fins on pressure drop; (**c**) Influence of different A_{sf} values of straight fins on outlet temperature; (**d**) Influence of different A_{sf} values of serrated fins on outlet temperature.

From Equation (1), a^* increases as h decreases or s increases. As observed in Figure 4, it can be seen that under the same Re, both in laminar- and turbulent-flow conditions, the pressure drop for straight fins and serrated fins decreases with the increase in a^*, and the outlet temperature decreases with the decrease in A_{sf}. This observation can be attributed to the fact that for the same Re, increasing a^* results in a larger windward area of the fins, which, in turn, leads to reduced flow velocity and, consequently, a decreased pressure drop. Reducing A_{sf} implies a smaller proportion of heat-transfer area (A) between the fluid and solid, resulting in an overall reduction in heat transfer under the same conditions and, subsequently, a decrease in outlet temperature. This is further validation of the model's reliability.

4. Results and Discussion

This research has analyzed and summarized the influence of geometric parameters and flow conditions on the application of the PM approach to equivalent flow and heat transfer in straight fins and serrated fins. A quantitative comparison has been made between the actual model and the PM model. Figure 6 demonstrates the effect of various straight-fin geometries on flow characteristics, and Figure 7 demonstrates the effect of various serrated-fin geometries on flow characteristics. Figures 8 and 9 illustrate the impact of various straight-fin geometries on heat-transfer properties, and Figure 10 illustrates the impact of different serrated-fin geometries on heat-transfer characteristics.

$$\delta = \frac{|x - \mu|}{x} \times 100\% \tag{14}$$

In the formulas, δ_f represents the flow error; δ_s represents the heat-transfer error; x stands for the actual value, Pa/K; and μ represents the approximate value, Pa/K. In this study, x represents the pressure drop and outlet temperature values of the fin models,

while μ represents the pressure drop values and simulated outlet temperature values of the PM model.

4.1. Effect of Geometric Parameters on Flow

4.1.1. Straight Fins

The influence of fin geometry on the flow is represented by the effect of different aspect ratios (a^*) and Reynolds numbers (Re) on the flow error. As shown in Equation (14), the flow error of the fins is obtained by calculating the difference between the mean pressure difference between the inlet and outlet surfaces of the PM method and the mean pressure difference between the inlet and outlet surfaces of the actual model.

As seen in Figure 6, for the same Re, flow errors increase as the a^* value rises. The flow error in laminar and turbulent flow with a straight-fin aspect ratio of 0.98 reaches up to 70% and 55%; in contrast, the flow error in laminar and turbulent flow with a straight-fin aspect ratio of 0.17 is within 5%. The reason for this phenomenon is that a lower aspect ratio results in a smaller fin size that is closer to a more realistic PM, thus leading to higher accuracy.

From the overlap of the curves at different Reynolds numbers in Figure 6b, it can be observed that the higher the Re, the closer the curves are, and the smaller the effect of the change in Re on the pressure-drop error. When comparing the error ranges caused by both a^* and Re, the maximum variation in flow error within Re values ranging from 200 to 1000 is around 10%. However, within a^* values from 0.05 to 0.98, the maximum variation in flow error reaches 70%. Clearly, a^* exhibits a more significant impact relative to Re on the error.

For straight fins, when the aspect ratio satisfies $0 < a^* < 0.17$ for laminar flow at $200 < \mathrm{Re} < 1000$ and turbulent flow at $1200 < Re < 5000$, the flow error generated by the PM method is within 15%.

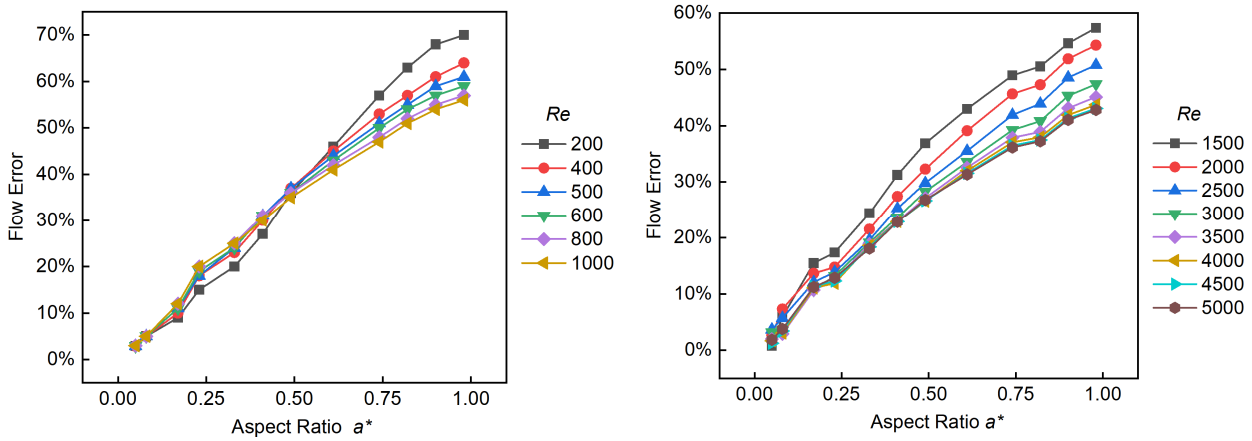

Figure 6. Influence of different aspect ratios (a^*) of straight fins on flow error: (**a**) Laminar-flow state; (**b**) Turbulent-flow state.

4.1.2. Serrated Fins

As for serrated fins, the effect of a^* on the flow error followed the same rule. As shown in Figure 7, under the same Re conditions, the flow error (δ_f) decreases as a^* decreases. Furthermore, when comparing the error ranges for straight fins and serrated fins in Figures 6 and 8, it is clear that the effect of Re is more significant for straight fins compared with serrated fins.

As shown in Figure 7a, the flow error increases significantly at an Re of 200. It is analyzed that at a low Reynolds number, the porous medium is mainly controlled by viscous forces, and the inertial resistance can be neglected. The flow law can be described by Darcy's law, which states that the flow velocity of the fluid is linearly proportional to the pressure difference. As shown in Figure 7b, in the Re range of 1000–2000, the flow over

serrated fins could reside in the transition zone, causing inaccuracies when employing turbulence modeling.

For serrated fins, when the aspect ratio satisfies $0 < a^* < 0.28$ for laminar flow at $400 < Re < 1000$, and when the aspect ratio satisfies $0 < a^* < 0.29$ for turbulent flow at $1200 < Re < 5000$, the flow error generated by the PM method is within 15%. However, Figures 6 and 7 demonstrate that, within the computational range of this study, for straight fins at $0.17 < a^* < 0.98$ and serrated fins at $0.29 < a^* < 0.68$, the flow errors generated by employing the PM method exceed 15%. Further correction of the equivalent resistance coefficients is required.

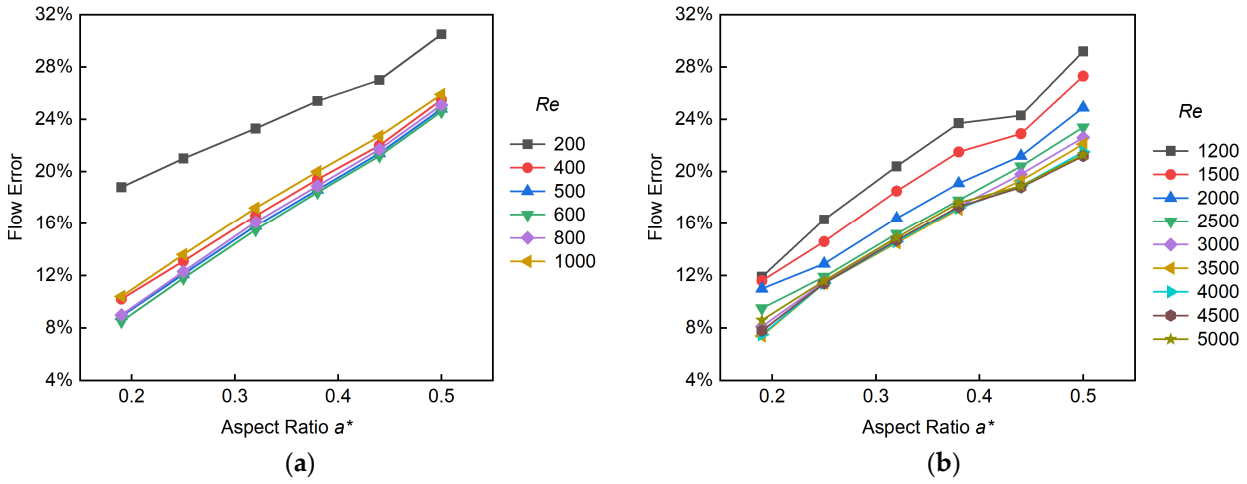

Figure 7. Influence of different aspect ratios (a^*) of serrated fins on flow error: (**a**) Laminar-flow state; (**b**) Turbulent-flow state.

4.2. Effect of Geometric Parameters on Heat Transfer

4.2.1. Straight Fins

The influence of fin geometry on heat transfer is represented by the effect of different porosity (γ) and specific surface area (A_{sf}) values on the heat-transfer error. As shown in Equation (14), the heat-transfer error of the fins is obtained by calculating the difference between the mean temperature of the outlet surface of the PM method and the mean temperature of the outlet surface of the actual model.

Figure 8 shows that for straight fins, whether in laminar or turbulent flow, the heat-transfer errors (δ_h) using the PM approach remain within 8%. This indicates that the results of the PM non-equilibrium method closely match those of the actual model.

Figures 8a and 9a clearly illustrate that heat-transfer errors (δ_h) diminish with decreasing γ at identical Re conditions. This is due to γ defining the ratio of the fluid-flow volume to the porous-area volume. Diminished γ values signify larger solid volumes, thereby augmenting heat conduction through the solid material. As the fin reaches thermal equilibrium, heat diffusion becomes more uniform, resembling the heat diffusion pattern observed in the PM model. Consequently, fewer discrepancies arise between the results derived from the PM approach and those generated by the actual model.

Figures 8b and 9b illustrate that heat-transfer errors (δ_h) decrease with increasing A_{sf} at identical Re conditions. A_{sf} signifies the ratio of the fluid–solid interface area to the PM area volume. An elevated area density indicates a larger fluid–solid interface area, expanding the heat-transfer region. Subsequently, external heat transfer to the fins is enhanced, which promotes the uniformity of heat transfer within the fin models.

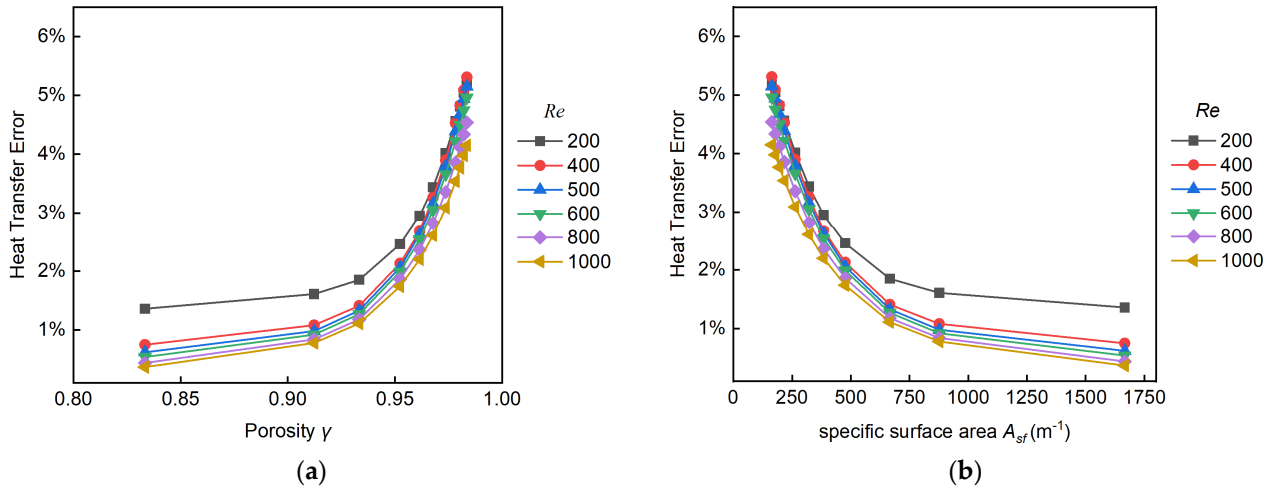

Figure 8. Influence of flow error on different geometrical structures of laminar straight fins: (**a**) Effect of different porosities γ; (**b**) Effect of different interfacial area densities $A_{sf.}$

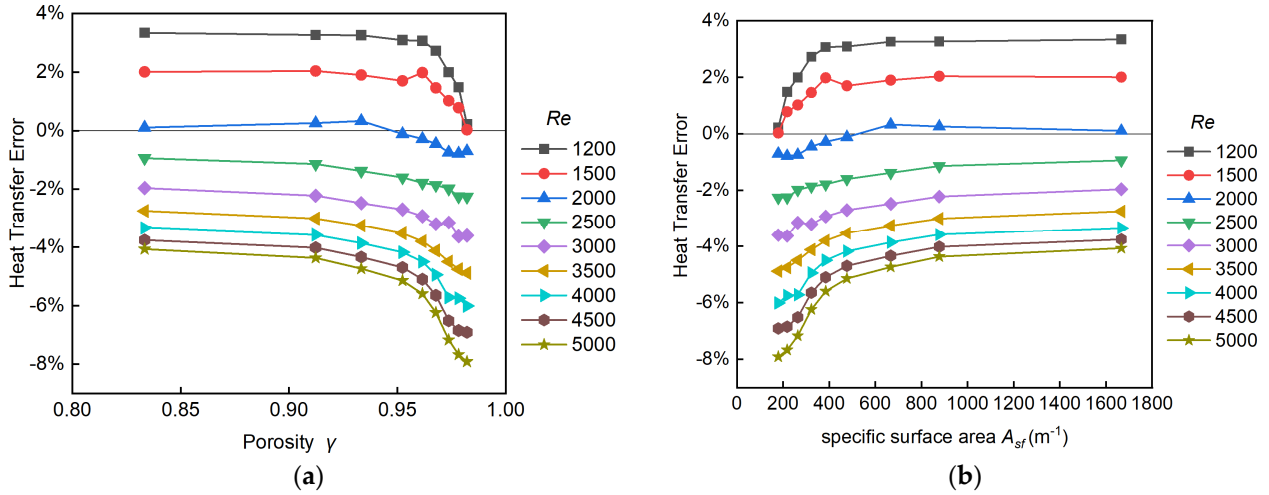

Figure 9. Influence of flow error on different geometrical structures of turbulent straight fins: (**a**) Effect of different porosities γ; (**b**) Effect of different interfacial area densities $A_{sf.}$

4.2.2. Serrated Fins

As shown in Figure 10, for serrated fins, δ_h decreases with increasing A_{sf} for the same *Re*. The heat-transfer error employing the PM approach remains within 10% for both laminar and turbulent flow. Based on the above results, the effects of A_{sf} on heat transfer in serrated fins are the same as those in straight fins, which further validates the versatility of the PM method for fins.

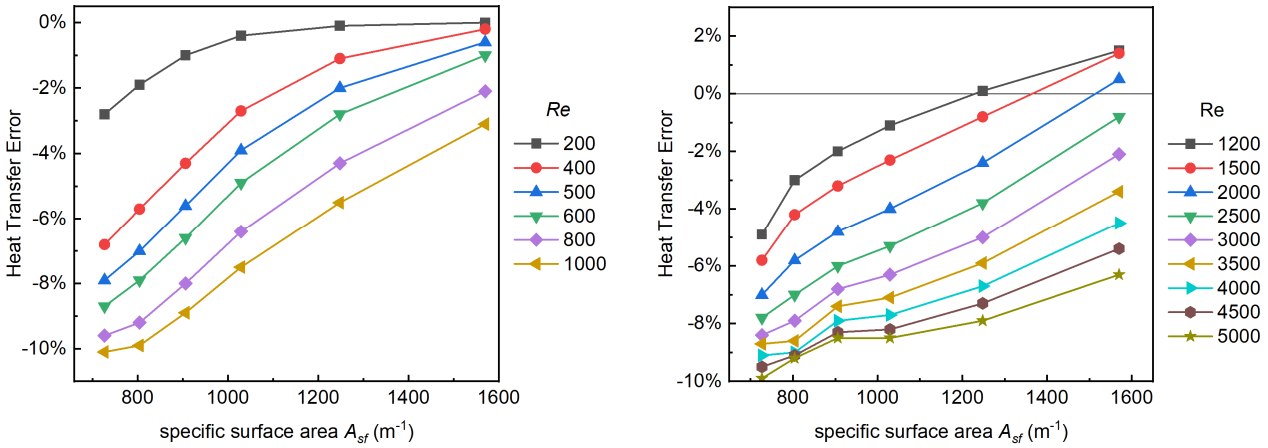

Figure 10. Influence of different specific surface area (A_{sf}) values of serrated fins on flow error: (**a**) Laminar-flow state; (**b**) Turbulent-flow state.

5. Conclusions

In this study, we conducted a validation analysis of the PM method for straight fins and serrated fins, exploring various geometric parameters, including the aspect ratio (a^*), specific surface area (A_{sf}), and porosity (γ), to understand their influence on the application of the PM approach under different flow conditions. The results showed the following:

1. The flow errors (δ_f) introduced by the application of the PM approach increase with an increase in the aspect ratio (a^*). In the case of straight fins, under laminar and turbulent flow, δ_f can reach as high as 45% when a^* is 0.98, while δ_f remains below 5% for an a^* value of 0.17.
2. The heat-transfer errors (δ_h) introduced by the application of the PM approach increase with a decrease in A_{sf} and an increase in γ. For both straight fins and serrated fins with a range of porosity from 0.8 to 1, δ_s is less than 15%.
3. For straight fins at $0 < a^* < 0.17$ in the laminar regime ($200 < Re < 1000$) and in the turbulent regime ($1200 < Re < 5000$), and for serrated fins at $0 < a^* < 0.32$ in the laminar regime ($400 < Re < 1000$) or at $0 < a^* < 0.28$ n the turbulent regime ($2000 < Re < 5000$), both δ_f and δ_h resulting from employing the PM approach are within the accepted range.

Author Contributions: Conceptualization, J.T. and S.L.; methodology, J.T. and S.L.; validation, S.L.; investigation, S.L.; resources, J.T., S.L. and T.W.; data curation, S.L. and J.T.; writing—original draft preparation, S.L.; writing—review and editing, J.T., S.L., T.W., S.W. and H.X.; visualization, S.L. and S.Y.; supervision, J.T., T.W., S.W. and H.X.; project administration, J.T., T.W. and H.X.; funding acquisition, J.T. and T.W. All authors have read and agreed to the published version of the manuscript.

Funding: This research was funded by the Research Ability Improvement Project of Key Construction Subjects in Guangdong Province (grant number 2021ZDJS061), the Basic and Applied Basic Research Fund Project of Guangdong Province (grant number 2022A1515110911), the Young Talent Research Project of the Guangzhou Education Bureau College Research Project (grant number 202234600), and the First-class Curriculum Project of Guangzhou Universities (grant number 2023YLKC038).

Data Availability Statement: The data presented in this study are available on request from the corresponding author. The data are not publicly available due to the value of further research..

Conflicts of Interest: The authors declare no conflict of interest.

References

1. Careri, F.; Khan, R.H.U.; Todd, C.; Attallah, M.M. Additive manufacturing of heat exchangers in aerospace applications: A review. *Appl. Therm. Eng.* **2023**, *235*, 121387. [CrossRef]
2. Liu, Z.; Sun, M.; Huang, Y.; Li, K.; Wang, C. Investigation of heat transfer characteristics of high-altitude intercooler for piston aero-engine based on multi-scale coupling method. *Int. J. Heat Mass Transf.* **2020**, *156*, 119898. [CrossRef]
3. Chen, M.; Sun, X.; Christensen, R.N. Thermal-hydraulic performance of printed circuit heat exchangers with zigzag flow channels. *Int. J. Heat Mass Transf.* **2019**, *130*, 356–367. [CrossRef]
4. Ponangi, B.R.; Krishna, V.; Seetharamu, K.N. Performance of compact heat exchanger in the presence of novel hybrid graphene nanofluids. *Int. J. Therm. Sci.* **2021**, *165*, 106925. [CrossRef]
5. Yoon, S.-J.; O'Brien, J.; Chen, M.; Sabharwall, P.; Sun, X. Development and validation of Nusselt number and friction factor correlations for laminar flow in semi-circular zigzag channel of printed circuit heat exchanger. *Appl. Therm. Eng.* **2017**, *123*, 1327–1344. [CrossRef]
6. Vaisi, A.; Javaherdeh, K.; Moosavi, R. Condensation heat transfer performance in multi-fluid compact heat exchangers with wavy and strip fins. *Int. J. Heat Mass Transf.* **2022**, *182*, 121968. [CrossRef]
7. Fang, W.; Chen, S.; Xu, J.; Zeng, K. Predicting heat transfer coefficient of a shell-and-plate, moving packed-bed particle-to-sCO2 heat exchanger for concentrating solar power. *Energy* **2021**, *217*, 119389. [CrossRef]
8. Merchán, R.P.; Santos, M.J.; Medina, A.; Hernández, A.C. High temperature central tower plants for concentrated solar power: 2021 overview. *Renew. Sustain. Energy Rev.* **2022**, *155*, 111828. [CrossRef]
9. Yang, J.; Ma, L.; Bock, J.; Jacobi, A.M.; Liu, W. A comparison of four numerical modeling approaches for enhanced shell-and-tube heat exchangers with experimental validation. *Appl. Therm. Eng.* **2014**, *65*, 369–383. [CrossRef]
10. Pizzolato, A.; Sharma, A.; Maute, K.; Sciacovelli, A.; Verda, V. Multi-scale topology optimization of multi-material structures with controllable geometric complexity—Applications to heat transfer problems. *Comput. Methods Appl. Mech. Eng.* **2019**, *357*, 112552. [CrossRef]
11. Ciuffini, A.; Scattina, A.; Carena, F.; Roberti, M.; Rivalta, G.T.; Chiavazzo, E.; Fasano, M.; Asinari, P. Multiscale computational fluid dynamics methodology for predicting thermal performance of compact heat exchangers. *J. Heat Transf.* **2016**, *138*, 071801. [CrossRef]
12. Patankar, S.V.; Spalding, D.B. Computer analysis of the three-dimensional flow and heat transfer in a steam generator. In *Numerical Prediction of Flow, Heat Transfer, Turbulence and Combustion*; Pergamon: Oxford, UK, 1983; pp. 293–298.
13. Prithiviraj, M.; Andrews, M.J. Comparison of a three-dimensional numerical model with existing methods for prediction of flow in shell-and-tube heat exchangers. *Heat Transf. Eng.* **1999**, *20*, 15–19.
14. Hu, C.; Sun, M.; Xie, Z.; Yang, L.; Song, Y.; Tang, D.; Zhao, J. Numerical simulation on the forced convection heat transfer of porous medium for turbine engine heat exchanger applications. *Appl. Therm. Eng.* **2020**, *180*, 115845. [CrossRef]
15. Moradi, I.; Karimipour, A.; Afrand, M.; Li, Z.; Bach, Q.-V. Three-dimensional numerical simulation of external fluid flow and heat transfer of a heat exchanger in a wind tunnel using porous media model. *J. Therm. Anal. Calorim.* **2020**, *141*, 1647–1667. [CrossRef]
16. Man, Y.; Tong, J.; Wang, T.; Wang, S.; Xu, H. Study on Intermittent Microwave Convective Drying Characteristics and Flow Field of Porous Media Food. *Energies* **2022**, *16*, 441. [CrossRef]
17. Torresi, M.; Saponaro, A.; Camporeale, S.M.; Fortunato, B. CFD analysis of the flow through tube banks of HRSG. In *Turbo Expo: Power for Land, Sea, and Air*; The ASME: Berlin, Germany, 2008; Volume 43178, pp. 327–337.
18. William, T.S. An overview on rod-bundle thermal-hydraulic analysis. *Nucl. Eng. Des.* **1980**, *62*, 1–24.
19. Ismail, L.S.; Ranganayakulu, C.; Shah, R.K. Numerical study of flow patterns of compact plate-fin heat exchangers and generation of design data for offset and wavy fins. *Int. J. Heat Mass Transf.* **2009**, *52*, 3972–3983. [CrossRef]
20. Ahlinder, S. *On Modelling of Compact Tube Bundle Heat Exchangers as Porous Media for Recuperated Gas Turbine Engine Applications*; BTU Cottbus-Senftenberg: Brandenburg, Germany, 2006.
21. Li, Z.; Ding, Y.; Liao, Q.; Cheng, M.; Zhu, X. An approach based on the porous media model for numerical simulation of 3D finned-tubes heat exchanger. *Int. J. Heat Mass Transf.* **2021**, *173*, 121226. [CrossRef]
22. Zhu, Q.; Pishahang, M.; Caccia, M.; Kelsall, C.C.; LaPotin, A.; Sandhage, K.H.; Henry, A. Validation of the Porous Medium Approximation for Hydrodynamics Analysis in Compact Heat Exchangers. *J. Fluids Eng.* **2022**, *144*, 081403. [CrossRef]
23. Lage, J.L.; Antohe, B.V. Darcy's experiments and the deviation to nonlinear flow regime. *J. Fluids Eng.* **2000**, *122*, 619–625. [CrossRef]
24. Wilson, L.; Narasimhan, A.; Venkateshan, S.P. Turbulent flow hydrodynamic experiments in near-compact heat exchanger models with aligned tubes. *J. Fluids Eng.* **2004**, *126*, 990–996. [CrossRef]
25. Huang, Y.; Liu, Z.; Lu, G.; Yu, X. Multi-scale thermal analysis approach for the typical heat exchanger in automotive cooling systems. *Int. Commun. Heat Mass Transf.* **2014**, *59*, 75–87. [CrossRef]
26. Liu, Y.; Yu, C.; Qin, S.; Wang, X.; Lou, J. Effect of transverse flow in porous medium on heat exchanger simulation optimization. *Trans. Can. Soc. Mech. Eng.* **2020**, *44*, 419–426. [CrossRef]
27. Kays, W.M.; London, A.L. *Compact Heat Exchangers*; MEDTECH, Scientific International: New Delhi, IL, USA, 1984.
28. Wen, J.; Yang, H.; Tong, X.; Li, K.; Wang, S.; Li, Y. Optimization investigation on configuration parameters of serrated fin in plate-fin heat exchanger using genetic algorithm. *Int. J. Therm. Sci.* **2016**, *101*, 116–125. [CrossRef]

29. Yang, Y.; Li, Y. General prediction of the thermal hydraulic performance for plate-fin heat exchanger with offset strip fins. *Int. J. Heat Mass Transf.* **2014**, *78*, 860–870. [CrossRef]
30. Lam, C.K.G.; Sharmahorst, K.A. Modified Form of the k-εModel for Predicting Wall Turbulence. *J. Fluids Eng.* **1981**, *103*, 456–460. [CrossRef]
31. Liu, W.; Fan, A.; Huang, X. *Theory and Application of Heat and Mass Transfer in Porous Media*; Science Press: Beijing, China, 2006.
32. Li, H.; Zhang, X.; He, F. Numerical simulation of fluid flow in porous media. *J. Univ. Pet. Nat. Sci. Ed.* **2000**, *24*, 111–116.
33. Pan, H. Numerical Calculation of Darcy-Forchheimer Seepage in Porous Media. Ph.D. Thesis, Shandong University, Ji'nan, China, 2012.
34. Patankar, S.V.; Liu, C.H.; Sparrow, E.M. Fully developed flow and heat transfer in ducts having streamwise-periodic variations of cross-sectional area. *J. Heat Transf.* **1977**, *99*, 180–186. [CrossRef]